Pan American Advanced Studies Institute on

Transmission Electron Microscopy in Materials Science

July 2006, Santiago, Chile

EQUILIBRIUM VERSUS DISEQUILIBRIUM. A HR-TEM OVERVIEW IN HIGH-T METAMORPHIC PETROLOGY.

Dr. Diego MORATA

Dpto de Geología. Fac. Cs Físicas y Matemáticas.

Universidad de Chile

dmorata@cec.uchile.cl

METAMORPHISM

from the Greek "metamorphosis"

.... meaning change or alter form

Metamorphic Petrology is concerned with transformation that takes place in rocks in the solid state

These changes are due to physical and/or chemical conditions that differ from those normally occurring in the zone of weathering, cementation and diagenesis.

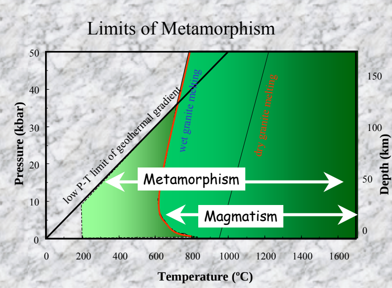

The limits of metamorphism are discussed with respect to temperature and pressure. The low-temperature limit of metamorphism is around 150 ± 50°C. According to the definition of metamorphism, the beginning of melting is included in the field of metamorphism as long as rocks remain predominantly in their solid state.

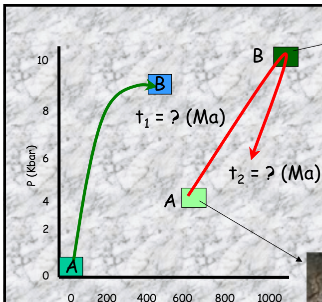

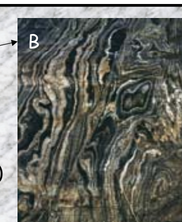

Metamorphic processes ocurred at a P-T-(X)-t values

Metamorphic processes can be viewed as a combination of:
(1) chemical reactions between minerals and between minerals and gases, liquids and fluids (mainly H_2O) and
(2) transport and exchange of substances and heat between domains where such reactions take place.

Consequently, an advanced understanding of metamorphism requires a great deal of insight into the quantitative description of chemical reactions and chemical transport processes, especially reversible and irreversible chemical thermodynamics.

The term metamorphism at it is related to processes, changes and reactions clearly also includes the aspect of time.

For a metamorphic reaction (e.g. Ab ⇔ Jd + Qtz),

$$NaAlSiO_3 \Leftrightarrow NaAlSi_2O_6 + SiO_2$$

because

$\Delta G = -RT\ln K$ and $\Delta G = \Delta H - T\Delta S + \Delta VP$

at equilibrium P and T, the Gibbs free energy can be written as follows:

$$\Delta G_{(P,T,X)} = \Delta H^o + \int_{298}^{T} \Delta Cp/dt + \int_{1}^{P} \Delta V dP - T\{\Delta S^o + \int_{298}^{T} Cp/T\, dT\} + RT\ln K$$

Assuming that the heat capacity change of the reaction (ΔCp) is nearly zero and also that in such exchange reaction involving solid phases ΔV is nearly constant, the equilibrium reaction reduces to the following:

$$\Delta H^o - T\Delta S^o + \Delta V(P-1) + RT\ln K = \Delta G = 0$$

$NaAlSiO_3 \Leftrightarrow NaAlSi_2O_6 + SiO_2$

and for this reaction

$$K = \frac{[a]_{Jd}^{Px}\ [a]_{Qtz}}{[a]_{Ab}^{Pl}}$$

With $[a]_{Jd}^{Px} = X_{Jd}^{Px}\ \gamma$; being $X_{Jd}^{Px} = \frac{n_{Jd}}{\Sigma n_{Px}}$

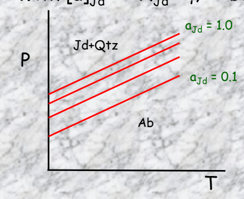

We need to know exactly the chemical composition (microanalyses) of minerals involved in a metamorphic reaction (and resolve the solid solution model!!!)

Them, a metamorphic rock can be considered as the consequence of a series of metamorphic reactions giving stable assemblages which cannot be distinguished from metastable ones by any petrographic technique, and metastable equilibria cannot be separated from stable equilibria.

One metamorphic assemblage can be considered in equilibrium when:
1.- the number of phases (Φ) present is controlled by the Gibbs phases rule (Φ + F = C+2)*;
2.- the system is chemically homogenised (absence of chemical differences between different regions of a system);
3.- absence of chemical differences at the scale of a same mineral
4.- minimal energy excess (reduction of grain size with orientation for optimised energy).

*In Petrology, C = SiO_2, Al_2O_3, MgO, FeO, CaO, Na_2O, K_2O, H_2O, (TiO_2, Fe_2O_3)

scale of equilibrium?

Microdomains:

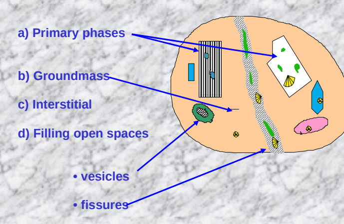

Different effective chemical composition ⇒ mineral chemistry

And metamorphic processes imply time!!

Geochronology based on isotopic systems

General ecuation:

$N_t = N_0\, e^{-\lambda t}$ → $D_t = D_0 + N_t\,(e^{\lambda t} - 1)$

For the $^{40}Ar/^{39}Ar$:

$$t = \frac{1}{\lambda} \ln\left(1 + J \times \frac{^{40}Ar_K{}^*}{^{39}Ar_K}\right)$$

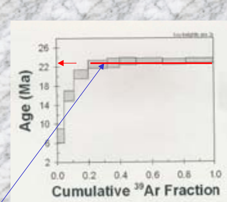

For a mineral with homogeneous Ar distribution, $^{40}Ar_K{}^*/^{39}Ar_K$ ratio would be constant along the mineral at different temperatures → *plateau age*

However, some criteria and methods to detect disequilibrium in rocks do exist.

Disequilibrium Textures

Mineral reactions that are unable to proceed to completion leave a rock in a state of chemical disequilibrium which, on the scale of a thin section, may be indicative by a variety of disequilibrium textures.

Coronas (and reaction rims)

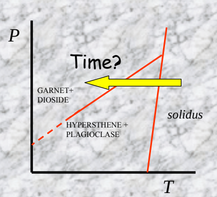

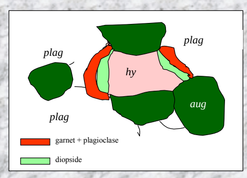

Exsolution

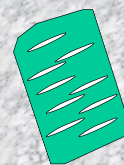

two inmiscible phases

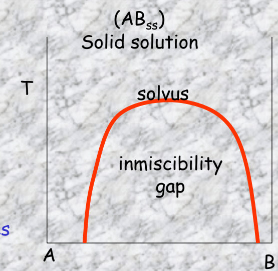

Zonning

heterogenous distribution of Ar in K-rich minerals and its influence in the $^{40}Ar/^{39}Ar$ geochronology

- All these textures which evidence disequilibrium can be studied using HR-TEM. In fact, the use of HR-TEM begin to be normally accepted by Metamorphic Petrologist to understand metamorphic reactions at a more detailed scale.
- Some Scientific Journals with HR-TEM works (Am. Mineral., EJM, CMP, Clay Min., Clay and Clay Min., Min. Mag., etc:)

Case of studies

With increasing the metamorphic grade

- Mica interlayering in low-grade mylonites
- Reaction coronas in mafic granulitic rocks
- Exsolution of hydrous minerals in clinopyroxenes from UHP rocks

Interpreting radiometric ages

- Chlorite interlayering in biotite (effect on Ar/Ar geochronology)

I- Mica interlayering in low-grade mylonites

(Arancibia & Morata, J.Str. Geol., 2005)

Mylonite: cohesive, foliated and usually lineated rock produced by tectonic grain-size reduction via crystal-plastic processes in narrow zones of intense deformation

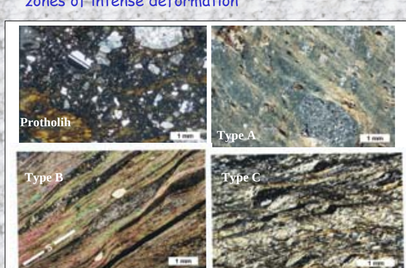

Sequence of relative *strain*

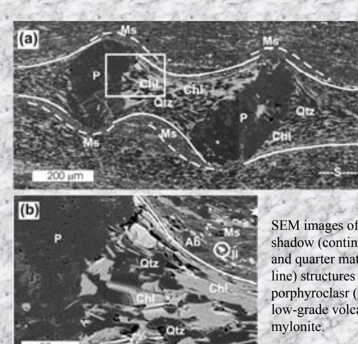

SEM images of pressure shadow (continuous line) and quarter mat (dotted line) structures around a porphyroclasr (P) in a low-grade volcanic mylonite.

White-mica composition in the mylonites

Mechanism of Ms formation (softening reactions: Ab⇔Ms + Qtz; KFd⇔Ms+Qtz):

$$3NaAlSi_3O_8 + K^+ + 2H^+ \Leftrightarrow KAl_3Si_3O_{10}(OH)_2 + 6SiO_2 + 3Na^+$$

$$3KAlSi_3O_8 + 2H^+ \Leftrightarrow KAl_3Si_3O_{10}(OH)_2 + 6SiO_2 + 2K^+$$

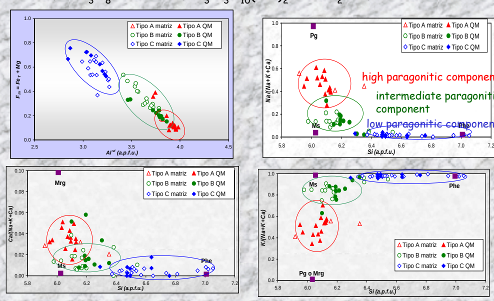

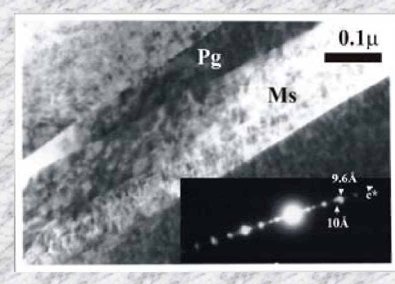

Low-magnification HR-TEM image of white-mica quarter mats showing fine paragonite (Pg) muscovite (Ms) interlayering. The SAED pattern shows the 10 Å (Ms) and 9.6 Å (Pg) periodicities indicating the Ms-Pg interlayering.

II- Reaction coronas in granulitic rocks

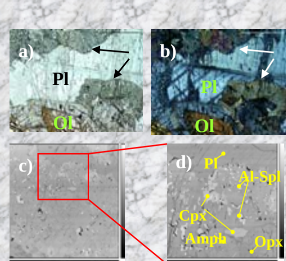

Sierra de La Huerta,
Western Pampean Ranges (Argentina)
(7-8 kbars, 860-930°C, 432±4 Ma)

Reaction coronas in granulitic rocks

(Mellini et al., 1983, Periodico di Mineralogia, 583-615)

Corona structures in a rock result from subsolidus transformations at relatively high pressure and temperature and consist of a sequence of layers which are indicative of subsequent reactions that took place among the various mineral phases due to changes in the environmental conditions.

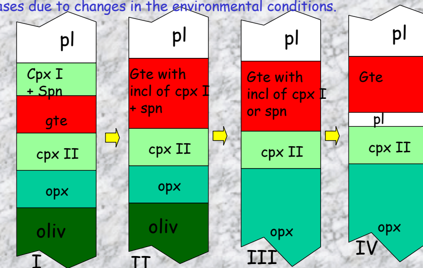

T > 900°C — 800°C < T < 900°C

Ol + Pl ⇒ Opx I+ Cpx I + Spn ⇒ Cpx II + Gte + Opx II

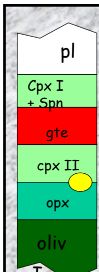

Orthopyroxene-Clinopyroxene inferface

Low-Al Cpx without relevant defective microstructures but nearby Opx highly altered by hydratation reactions with development of layer silicates and also amphibole.

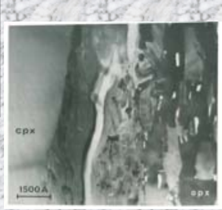

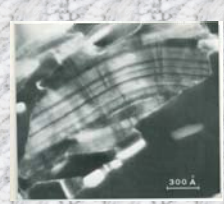

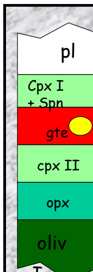

Clinopyroxene in the garnet zone

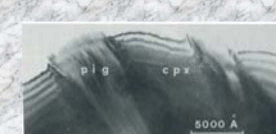

Low-Ca pyroxene (pigeonite) inclusion in the Cpx I $(Na_{0.2}Ca_{0.7}Mg_{0.8}Fe_{0.2}Al_{0.1})(Si_{1.7}Al_{0.3})O_8)$ from the garnet zone of the corona.

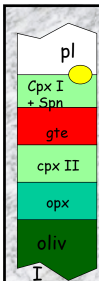

Garnet-Clinopyroxene inferface

Plagioclase (Ab46An54) and spinel ($(Mg_{0.6}Fe_{0.4})(Al_{1.9}Fe_{0.1})O_{4.0}$) inclusions in Cpx

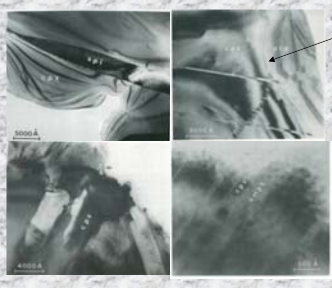

Interface Cpx-Pl cutted by tw faulted lamellae of spinel

Hydratation reactions with presence of 14 Å layer silicate or amphibole lamellae within the Cpx

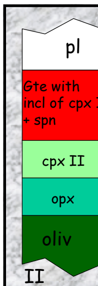

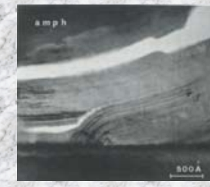

Opx heavly altered into layer-silicates

Amph cutted by faulted and folded layer silicate veinlet

Hydratation reactions

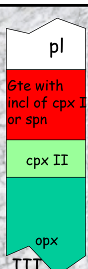

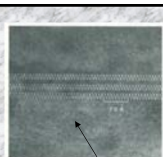

Cpx cutted by abundant (010) amphibole lamellae

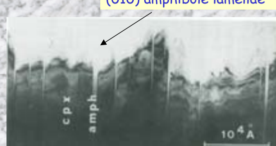

Conclusions

•HR-TEM images pointed out the presence of a relevant amount of amphiboles (and other more hydrated phases) in all the so-called "anhydrous" coronas.

•EMPA in Cpx of these coronas can be biased by the presence of amphibole lamellae (influence in the Jd/Ts ratios and in the Fe-Mg distribution between garnet and clinopyroxene ⇒ influence in the geothermobarometric calculations).

•Identification of amphibole structure allowing us to characterice different amphibolitation reactions (≠ P-T and partial water pressure conditions).

III- Exsolution of hydrous minerals in clinopyroxenes from UHP rocks. (Chen & Xu, 2005, EJM, 17, 895-903)

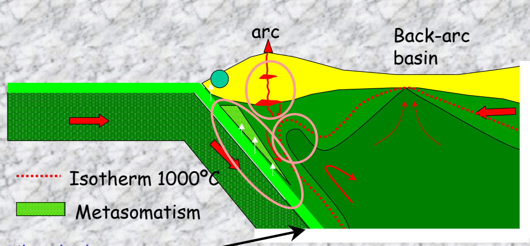

Ultra high-pressure

Deep subduction of crustal materials affects mantle convection and Earth dynmics and great amounts of water and potassium are transported into the deep mantle affecting the rheology of upper mantle rocks

Study of exsolution textures formed during exhumation of ultra high pressure (UHP) metamorphic rocks

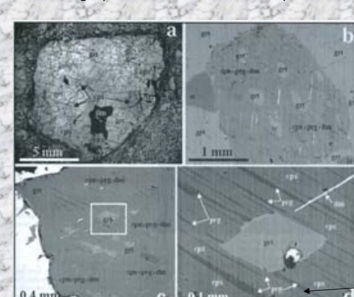

Primary rock: garnet pyroxenite (mantle xenoliths)

Origin of pargasite (hydrous mineral) exsolution in clynopyroxene (anhydrous mineral)?

Pargasite lamellae range from 1 to 10 μm

Presence of OH or hydrogen in the lattice of the normally anhydrous silicates prior to exsolution?

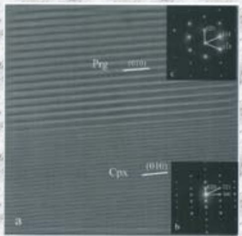

(a) HR-TEM image showing the planes of pargasite (Prg) (010) paralleling to planes of Cpx (010); (b) Selecte-area electron diffraction (SAED) patterns of pargasite; (c) SAED pattern of Cpx.

Compositional variations of pargasite exsolution lamellae from the garnet-pyroxenites (amphibole composition close to the pargasite end-member).

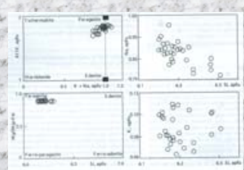

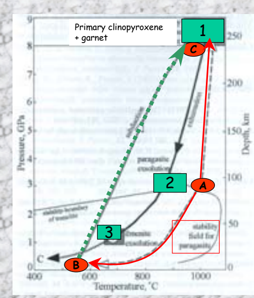

Possible P-T evolution of garnet-pyroxenites. The protolith garnet-pyroxenites were originated from the upper mantle (possible PT location in site A) and, as xenoliths, brought to crust level by magma uplift (from A to B) and them subducted to UHP metamorphic conditions (dotted path in green), or altenatively, direct dragged to a depper level by the subducted slab (from site A to C).

Mematorphic history (P-T-t path)

1. The peak of UHP metamorphism
2.- Clinopryroxene breakdown and pargasite exsolution
3.- Ilmenite exsolution

Conclusions:

- BSE and HR-TEM images indicate that composition of primary (pre-exsolution) clinopyroxene could be estimated by mixing of 10% pargasite and 90 % host pyroxene.
- Pargasite contains ≈2wt %H_2O (them, primary pryroxenes contains ≈ 2000 ppm H2O).
- HR-TEM images evidence that pargasites are aligned parallel to their host clinopyroxene lattice (primary origin for exsolution).
- Them, primary super-silicic pyroxenes were H_2O-bearing clinopyroxenes and and decomposed into two phases: dioside and pargasite.
- According HR-TEM evidences, pargasite exsolution lamellae represent an original (= primary) exsolution texture and consequently H_2O in pargsasite should be derived from primary H_2O-bearing clinopyroxene.
- Consequently, significant amount of H_2O are transported from the Earth's surface into the upper mantle during subduction (influence of water recycling processes in subduction zones in the genesis of magmas and earthquake).

IV- Chlorite interlayering in biotite (effect on Ar/Ar geochronology). (Di Vincenzo et al., CMP, 145, 643-658)

The use of biotite in ^{40}Ar–^{39}Ar geochronology is sometimes limited by the occurrence of discordant age-spectra that are difficult to interpret. Biotite age spectra can exhibit low ages in the low-temperature steps (<600 °C), which rise to a flat or near-flat region above ~600 °C. This feature was attributed to gas-release controlled by defect-enhanced diffusion mechanisms at low temperatures, coupled with $^{39}Ar_K$ re-distribution by recoil during neutron irradiation. These structural and textural variations can be documented at the submicroscopic scale using HR-TEM.
The disturbance of age spectra at temperatures above ~600 °C was attributed to sample heterogeneity [either the coexistence of two different biotites or the presence of interlayered chlorite], coupled with $^{39}Ar_K$ re-distribution by recoil during sample irradiation, and/or the presence of an excess argon component.

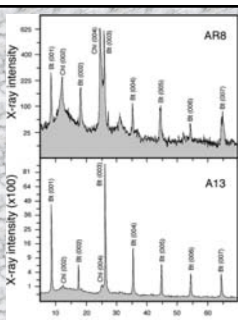

Studied samples belong to a medium- to coarse-grained biotite (± amphibole) two-feldspar granite (sample A13) and from a porphyritic (biotite ± amphibole) granite dyke (sample A18). U–Pb zircon data from both samples yielded ages of 490.8±6.2 and 484.5±8.7 Ma (±2) for samples A13 and AR8, respectively. At the microscopic scale, biotite in sample AR8 appears intensely chloritised. Pristine looking biotite grains are rare, whereas chlorite domains up to ~100–200 μm in size are common. Most biotite in sample A13 looks pristine. Rare chlorite domains, up to a few tens of microns thick, were observed in a few biotite grains.

XRD patterns of biotite separates used for incremental laser heating analyses. *00 l* reflections corresponding to biotite (Bt) and chlorite (Chl) are shown

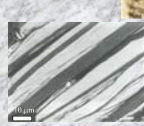

HR-TEM images

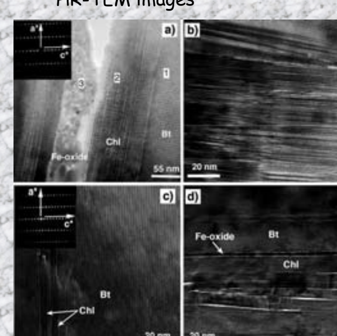

TEM images of untreated biotites from investigated samples. **a** Low magnification image of sample AR8 with *1* ordered biotite domains, *2* chlorite-rich domains and *3* poorly crystalline Fe-rich regions. The a*c* SAED (*inset*) is characterised by streaking along c*. **b** AR8 biotite, finely interlayered with chlorite. **c** Regular sequence of biotite 001 lattice fringes in sample A13 (10 Å spacing), with rare chlorite intercalations (14 Å spacing). The *inset figure* shows the corresponding a*c* SAED pattern (with no streaking). **d** Poorly crystalline Fe-oxide and chlorite associated with biotite A13. This image represents one of the most complex and altered regions observed in sample A13

Samples heated in vacuo

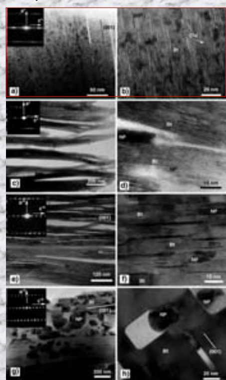

TEM investigation of the most chloritised biotite grains, heated in-vacuo, documented the complex decomposition and transformation process experienced by interlayered biotite-chlorite samples: (1) at ~600 °C, the deformation and bending of both biotite and chlorite, which is more advanced in chlorite, is coupled with a strong reduction of crystallinity in comparison with the untreated sample;

TEM images of the laser-heated biotite flake from sample AR8. **a** Sample after 0.3 W **(~600 °C)** heat-treatment. Delamination is absent. a*c* SAED pattern (*inset*) suggests significant loss of crystallinity. **b** Sample after 0.3 W heat treatment. Chlorite interlayered with biotite. Note the loss of contrast of the 14-Å lattice fringes due to chlorite decomposition.

Samples heated in vacuo

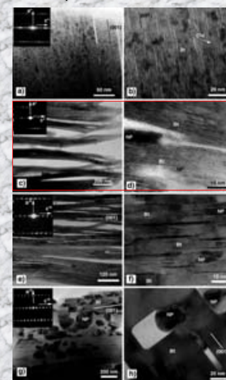

(2) at ~810 °C, the disappearance of the chlorite and the appearance of new phases along the (001) biotite planes is accompanied by the development of important delamination and the start of structural reorganisation of biotite;

c Sample after 0.7-W heat treatment, characterised by important delamination. a*c* SAED pattern of biotite (*inset*) reveals low crystallinity, but also poor streaking along c*. **d** Sample after 0.7 W (**~810 °C**) heat treatment showing biotite associated with new mineral phases (NP) derived from the breakdown of chlorite.

Samples heated in vacuo

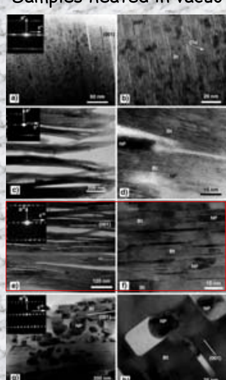

e Sample after 1.2 W heat treatment showing reduced delamination. a*c* pattern of biotite (*inset*) suggests structural reorganisation (intense reflections, no streaking along c*). **f** Typical nanotexture of sample after 1.2 W (**~940 °C**) heat treatment, highly crystalline biotite lamellae (up to 15–20 nm thick) and new mineral phases (NP).

(3) at ~940 °C, the retrogression of the delamination is associated with an advanced structural reorganisation of biotite (i.e. increased crystallinity);

Samples heated in vacuo

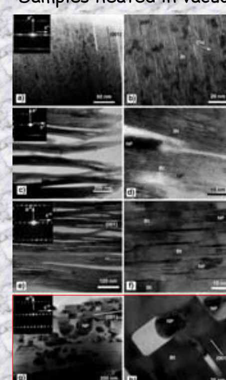

g Sample after 2.2 W (**~1,080 °C**) heat treatment. *Dark grains* are neoformed phases (NP) within highly crystalline biotite (light grey matrix). a*c* SAED pattern (*inset*) shows very intense and sharp reflections. **h** Typical nanotexture of sample after 2.2 W heat treatment. New phases (NP) are hosted within negative crystals

(4) >1,000 °C, development of a new nanotexture consisting of chlorite decomposition products hosted within euhedral, negative crystals of highly crystalline biotite

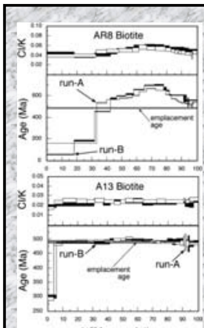

Age release and Cl/K spectra of biotites. Errors are 2. The *shaded areas* indicate the true emplacement age of the two samples based on U–Pb zircon data

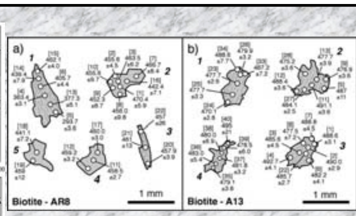

Line drawing showing the distribution of laser spot-fusion ages in biotite of samples AR8 and A13. *Numbers in brackets* reflect the data-sampling sequence in time . The rabdom distribution of $^{40}Ar/^{39}Ar$ spot ages whitin single biotite grains reflects the heterogeneous distribution of more or less intensely chloritised domains.

Comparison of the step-heating ages with spot fusion data (spatial distribution of Ar within biotite)

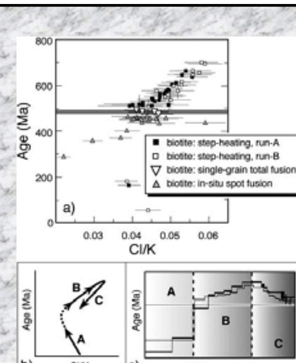

a ^{40}Ar–^{39}Ar ages plotted against Cl/K ratios derived from $^{38}Ar_{Cl}/^{39}Ar_{K}$ ratios for laser step-heating experiments on biotite sample AR8, including single-grain biotite total fusion and in situ spot-fusion analyses. The *shaded area* indicates the emplacement age of the AR8 dyke based on U–Pb zircon data. The *bold arrows* in **b** describe the observed trajectory of biotite age-steps with increasing temperature, and *A*, *B* and *C* denote the three temperature regions defined in text. In **c** the three temperature regions (*A*, *B*, *C*) are identified in the age spectra of biotite AR8.

Interpretation of the perturbed hump-shaped Ar/Ar age spectra with both anomalously young and old ages

Conclusions

- TEM investigation of the untreated biotite grains revealed the presence of chlorite interlayering ranging in thickness from tens of nanometres down to the unit-cell scale and extended defects, such as layer bendings and dislocations.
- The density of extended defects after irradiation may be even higher due to the possible development of irradiation-damage defects.
- TEM data on heated biotite samples have allowed the reconstruction of the evolution of the hump-shaped ^{40}Ar-^{39}Ar age spectra. The initial ascending segment (from low- to intermediate-temperatures) is ascribed to differential release of argon isotopes hosted in three main reservoirs. From the least to the most retentive, the reservoirs are (1) extended defects, enriched in recoiled $^{39}Ar_K$, (2) chlorite, enriched in recoiled $^{39}Ar_K$ and (3) biotite, depleted in recoiled $^{39}Ar_K$. The final descending segment of the age spectra is believed to be produced by argon released from progressively larger biotite domains in which $^{39}Ar_K$ recoil loss was less important.

General conclusions

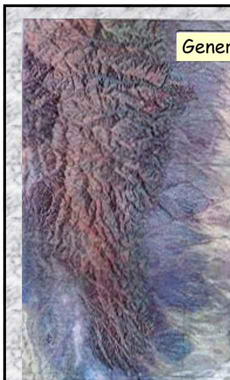

- In complex systems (e.g. metamorphism) thin section and EMPA are not sufficient to reveal the whole-rock complexity and therefore neglect a source of possible information.
- On the other hand, crystal-chemical arguments, which are based on site population and bond distance considerations resulting from accurate structure refinements, may be of great help in assigning or in supporting a genetic hypothesis for a particular phase.
- The deep understanding of the evolution of a rock has therefore to be founded on the combination of the results obtained from different approaches, even if each of them is able to give only qualitative or semi-quantitative indications.
- HR-TEM data greatly contribute to determine physical parameters on the history of the rocks.

The macro ⇔ micro cycle

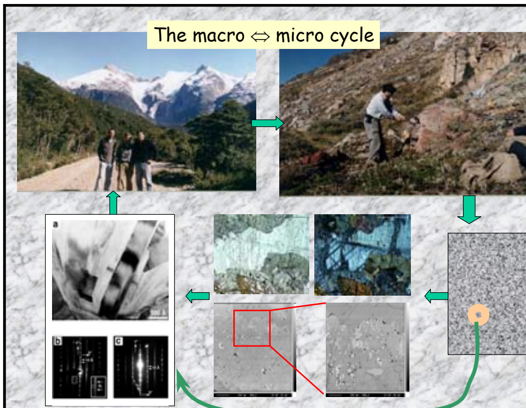

And
thank you very much
for your attention!